

# Electric-field-dependent spectroscopy of charge motion using a single-electron transistor

K. R. Brown,\* L. Sun, and B. E. Kane

Laboratory for Physical Sciences, 8050 Greenmead Drive, College Park, Maryland, 20740

We present observations of background charge fluctuators near an Al-AIO<sub>x</sub>-Al single-electron transistor on an oxidized Si substrate. The transistor design incorporates a heavily doped substrate and top gate, which allow for independent control of the substrate and transistor island potentials. Through controlled charging of the Si/SiO<sub>2</sub> interface we show that the fluctuators cannot reside in the Si layer or in the tunnel barriers. Combined with the large measured signal amplitude, this implies that the defects must be located very near the oxide surface.

Metal single-electron transistors (SETs) have generated interest recently for possible applications in quantum information processing,<sup>1</sup> nanoelectronics,<sup>2</sup> and fundamental sensing.<sup>3</sup> They are known to be sensitive electrometers with a charge noise around  $10^{-6} e/\sqrt{\text{Hz}}$ .<sup>4</sup> Nevertheless, SETs have not yet fulfilled their promise in many areas due to their broad  $1/f^\alpha$  noise spectrum and large background charge fluctuations. Identification and elimination of the sources of these nonidealities will be important for the fabrication of practical SET devices.

Several groups have attempted to isolate the source of noise in metal SETs.<sup>5,6,7,8,9,10,11</sup> Furlan and Lotkhov used a configuration with four surface gates to locate charge traps very near the island of an Al SET.<sup>5</sup> Buehler *et al.* used a two-gate geometry to study two-level fluctuations in their device and identified sources both near the surface and in the bulk substrate.<sup>6</sup> However, there is as yet no consensus for the dominant noise source in metal SETs. Of particular interest are fluctuators that become evident when large electric fields ( $\gtrsim 1$  kV/cm) are applied to an SET. This regime is particularly relevant for silicon quantum computing proposals<sup>1,12</sup> that rely on an SET for final state determination, for displacement detection with an SET,<sup>3,13</sup> and for future SET-based electronic devices such as memories.<sup>2,14</sup>

We have identified similar irregularities in Al-AIO<sub>x</sub>-Al SETs fabricated on oxidized Si substrates. These defects manifest themselves as peaks in the polarizability of the gate-island dielectric as a function of gate potential. They are present in every SET device we have measured to date. Through the use of a multiple gate geometry we have determined that the defects associated with these irregularities must lie above the substrate surface. Thus, they would seem to be a typical feature of Al-AIO<sub>x</sub>-Al SETs regardless of substrate.

Each of our devices consists of an Al-AIO<sub>x</sub>-Al single-electron transistor on an oxidized Si substrate. Figure 1 shows a scanning electron microscopy (SEM) micrograph of one device, a cross sectional schematic, and a band diagram of the device geometry. We intentionally make the leads of the SET wide so that the system is effectively three parallel plates, as shown schematically in Fig. 1(b), thereby making the electrostatics of the device easier to model. Electric fields from the top and bottom gates are confined for the most part above and below the SET, respectively.

Device fabrication begins with a nearly intrinsic Si wafer ( $\rho > 10$  k $\Omega$ -cm). The wafer is implanted with B at an energy of 500 keV and an areal density of  $2.5 \times 10^{14}$  /cm<sup>2</sup> to form the bottom gate. The peak acceptor density of  $6 \times 10^{18}$  /cm<sup>3</sup>, high

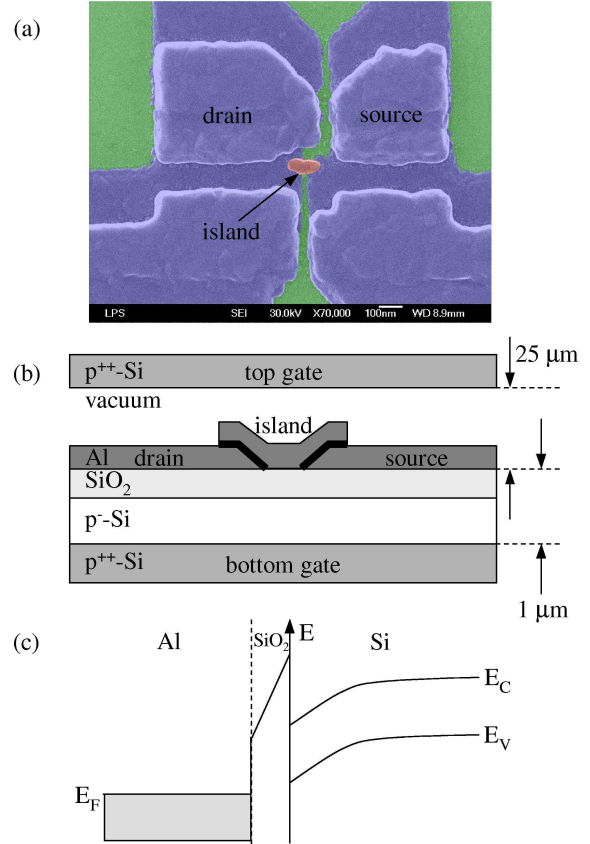


FIG. 1: (a) Colorized SEM micrograph of a typical device. Green areas represent the substrate, blue areas the SET leads, and the red area the SET island. The island dimensions are 60 nm × 130 nm, although only about half of this area is in contact with the substrate due to overlap with the leads. The leads extend farther than 600 nm from the island in any direction. (b) Cross sectional schematic of the SET geometry. The substrate is Si with 20 nm of surface thermal oxide. The Al source, island, and drain of the SET lie on the wafer surface. The heavily p-doped bottom gate has a peak density 1 μm below the surface. The top gate is suspended 25 μm above the chip. (c) Band diagram of the device in inversion. The electric field drives electrons toward the interface (left) and holes toward the substrate (right).

enough to conduct at low temperatures, occurs 1 μm below the surface. The wafer is then oxidized in a tube furnace at 950 °C to a thickness of 20 nm. We use electron-beam lithography and self-aligned double-angle evaporation to make the

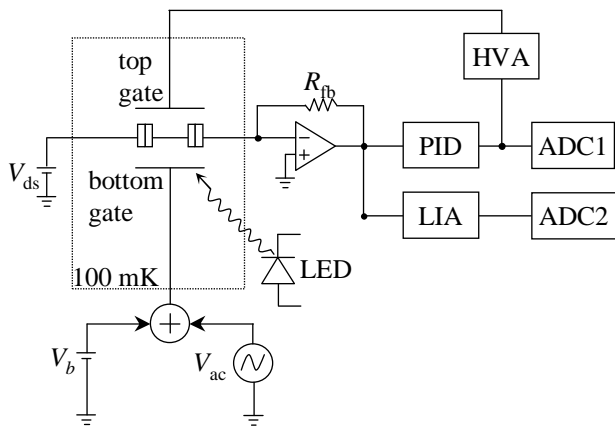


FIG. 2: Schematic of the measurement setup. LIA, lock-in amplifier; PID, proportional-integral-differential feedback; HVA, high-voltage amplifier; and ADC, analog-to-digital converter, respectively.

SETs.<sup>15</sup> The contact area between the SET island and substrate is of the order  $50 \times 50 \text{ nm}^2$ . The top gate consists of a piece of heavily doped Si, glued by hand to the wafer surface, but separated from it by  $25 \text{ }\mu\text{m}$  Kapton spacers at either end. The devices are cooled below 100 mK in an Oxford dilution refrigerator. A 1 T magnetic field is applied to keep them in the normal state.

Figure 2 shows a schematic of the measurement setup. For fixed drain-source bias  $V_{ds}$ , the current  $I_{ds}$  flowing through the device is monitored via a room-temperature current preamplifier with a 3 kHz bandwidth. As the potential  $V_b$  on the bottom gate is changed, a proportional-integral-differential (PID) feedback circuit maintains a constant  $I_{ds}$  by controlling the top gate voltage  $V_t$ , ensuring that the SET remains biased for maximum sensitivity. The feedback has a bandwidth of 10 Hz or less. To induce another electron onto the SET island using the top gate requires a voltage change around 60 V, so that a high-voltage amplifier (HVA) is required to amplify the output of the PID circuit into a useful range. A small ac dither  $V_{ac}$  at 1 kHz is applied simultaneously with  $V_b$  to the bottom gate, and the response of the SET at 1 kHz is measured with a lock-in amplifier (LIA). This signal is well above the 10 Hz bandwidth of the PID circuit, and so is unaffected by the latter. Both the PID output voltage, which reflects changes in the dc island potential, and the in-phase ac response (lock-in X channel) are then recorded while sweeping  $V_b$ . The setup includes an optical fiber to illuminate the sample with a light-emitting diode (LED) mounted at room temperature near the top of the refrigerator.

The response of the SET (as measured by the lock-in amplifier) to the ac dither  $V_{ac}$  on the bottom gate gives a measure of the polarizability of the intervening material. Figure 3(a) shows a typical trace of this polarizability versus bottom gate potential, where several peaks can be distinguished on a flat background. The data were acquired by sweeping the bottom gate voltage while countersweeping the top gate, thereby keeping a constant island potential. Presumably the peaks correspond to charges moving between distinct trapping sites when the gate potential  $V_b$  brings such sites into resonance.

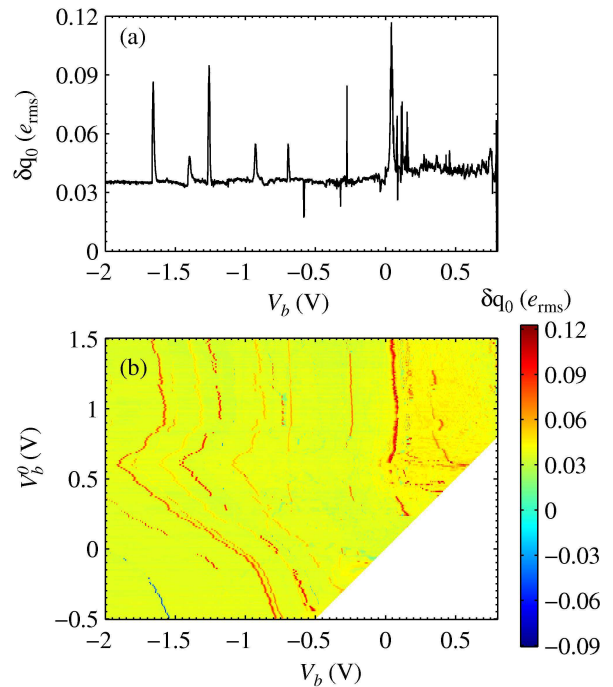


FIG. 3: (a) Polarizability  $\delta q_0$  as a function of bottom gate potential  $V_b$ . The data have been normalized to units of one electron on the SET island. (b) Polarizability  $\delta q_0$  (color of each point) as a function of bottom gate potential  $V_b$  and of charge at the interface, represented by the initial sweep voltage  $V_b^0$ .

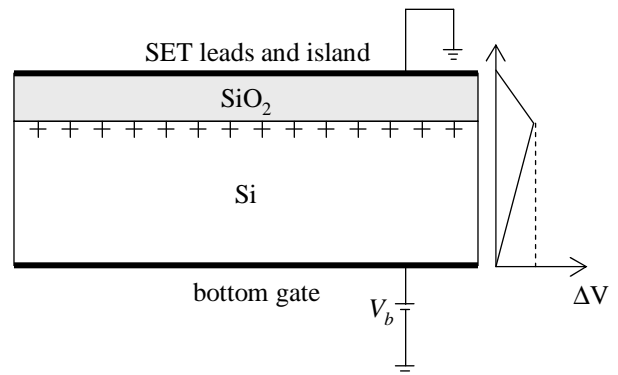


FIG. 4: Illustration of the effect of an increase in fixed positive charge at the Si/SiO<sub>2</sub> interface. The charge increases the electric field above the interface but decreases it below. This is illustrated by the diagram on the right, which shows the change in potential within the substrate induced by positive charge at the interface.

To glean some more information about these peaks, we place some charge at the Si/SiO<sub>2</sub> interface by biasing the bottom gate and illuminating the sample. The actual charging process is described in greater detail below. Such an interface charge leads to a potential drop across the interface, changing the electrostatic configuration as illustrated in Fig. 4. The resulting change in electric field within the substrate should shift a peak along the  $V_b$  axis in a direction determined by the defect's physical location, according to the following argument.

Consider the addition of some fixed charge to the interface that yields a change  $V_b^0$  in the potential there. To restore the electric field below the interface to its previous value requires a corresponding increase in the potential  $V_b$ . However, restoring the electric field above the interface instead necessitates an even larger *decrease* in  $V_b$ . If we assume that each peak occurs at a certain electric field, then the sign of  $dV_b/dV_b^0$  for a given peak locates its associated defect above or below the Si/SiO<sub>2</sub> interface.

To create an interface charge, a negative potential (-2.0 V) is applied to the bottom gate  $V_b$  (sufficient to strongly invert the surface), and the sample is illuminated. Referring to Fig. 1(c), illumination creates electron-hole pairs in the Si region. The holes flow out the bottom gate contact (to the right in the figure), while the electrons accumulate at the Si/SiO<sub>2</sub> interface. After illumination the bottom gate is returned to a higher potential  $V_b^0$ , removing some of the electrons from the interface, although all of the electrons are depleted only when  $V_b^0$  reaches approximately 0.5 V. Then  $V_b$  is swept back to -2.0 V while the polarizability is monitored, as discussed previously. Those electrons that have not been removed from the interface remain fixed during the sweep.

Figure 3(b) shows a sequence of such traces, each corresponding to a different value of  $V_b^0$ , now with the color of each point representing the polarizability. Here it is evident that the prominent peaks indeed are shifting along the  $V_b$  axis as  $V_b^0$  changes and charge is removed from the interface. Until  $V_b^0 \approx 0.6$  V, the slope  $dV_b^0/dV_b$  of these peaks is negative. A negative slope rules out the substrate beneath the Si/SiO<sub>2</sub> interface as the location of the defects, a conclusion supported by the realization that, for  $V_b^0 \lesssim 0.2$  V, there exists a two-dimensional electron gas at the interface. This electron gas should screen the SET island completely from any charge motion in the Si below, yet the peaks in polarizability persist in Fig. 3(b) for  $V_b^0 < 0.2$  V. The absence of an electron gas for  $V_b^0 > 0.2$  V also explains the slight increase of broadband noise here, as the SET becomes sensitive to a wider number of noise sources below the interface.

Beyond  $V_b^0 \approx 0.5$  V, all of the charge has been depleted from the interface, and the abrupt change in  $dV_b^0/dV_b$  near  $V_b^0 = 0.6$  V agrees with this value. Under such conditions we expect the peak positions to become independent of  $V_b^0$ , so that the slopes  $dV_b^0/dV_b$  should become nearly infinite. This is indeed the case for  $V_b^0 > 0.9$  V, but we note that several of the peaks acquire a positive slope for  $0.6 < V_b^0 < 0.9$  V. This positive slope is not presently understood, although we

suspect that it could be due to slow charge relaxation within the Si. For example, successive traces of  $\delta q_0(V_b)$  separated by a few minutes often show drifting of the peak positions, and in general the peak positions are stable only when care is taken to use identical initial conditions for successive traces. Positive  $dV_b^0/dV_b$  is consistent with a slow drift in time of the peaks toward larger values of  $V_b$ , because a given value for  $V_b$  occurs at later times relative to the start of the trace with increasing  $V_b^0$ .

To estimate the signal expected for a single charge moving in the substrate, we did a finite element analysis of our SET geometry using the FEMLAB physics modeling package. The analysis indicates that the maximum signal due to a single charge moving anywhere in the Si would be at most 0.09  $e$  rms, yet in Fig. 3 there are at least four peaks with magnitudes near this value. For charge motion within the SiO<sub>2</sub>, our analysis gives a sensitivity gradient of 0.037  $e$ /nm. A 0.09  $e$  rms signal therefore corresponds to a charge moving about 7 nm within the oxide, a distance we find implausible. Thus the signal magnitude indicates that the defects we observe lie not only above the Si but very near or above the oxide surface itself.

Defects within the tunnel barriers could easily lead to large charge offset signals. However, these defects are located between a lead held at constant potential and the SET island, also held at constant potential by the top gate and feedback circuit. The strong dependence of the observed peaks on the bottom gate voltage therefore rules out the tunnel barriers as their origin.

We have observed similar anomalies in seven SETs of this design, as well as in SETs fabricated on undoped Si substrates using surface gates. Thus they would seem to be typical features in Al-AlO<sub>x</sub>-Al SETs on oxidized Si substrates. We have excluded the Si, the SiO<sub>2</sub>, and the tunnel barriers as the location of the defects associated with these peaks. They must therefore reside very near the substrate surface. One possibility is that the peaks are associated with Al grains near the SET island. Many such isolated grains are clearly visible in magnified SEM images of our devices, although this hypothesis awaits further studies. Another group has observed excellent charge offset stability in Si-based SETs that should lack such grains,<sup>16</sup> an observation that may well support our conjecture. Future experiments to eliminate these grains are compelling in light of the importance of metal SETs to quantum information processing, nanoelectronics, and fundamental sensing.

This work was supported by the National Security Agency.

\* Electronic address: kbrown@lps.umd.edu

<sup>1</sup> B. E. Kane, N. S. McAlpine, A. S. Dzurak, R. G. Clark, G. J. Milburn, H. B. Sun, and H. Wiseman, Phys. Rev. B **61**, 2961 (2000).  
<sup>2</sup> H. Sunamura, T. Sakamoto, Y. Nakamura, H. Kawaura, J. S. Tsai, and T. Baba, Appl. Phys. Lett. **74**, 3555 (1999).  
<sup>3</sup> M. D. LaHaye, O. Buu, B. Camarota, and K. C. Schwab, Science **304**, 74 (2004).  
<sup>4</sup> A. Aassime, D. Gunnarsson, K. Bladh, P. Delsing, and

R. Schoelkopf, Appl. Phys. Lett. **79**, 4031 (2001).

<sup>5</sup> M. Furlan and S. V. Lotkhov, Phys. Rev. B **67**, 205313 (2003).

<sup>6</sup> T. M. Buehler, D. J. Reilly, R. P. Starrett, V. C. Chan, A. R. Hamilton, A. S. Dzurak, and R. G. Clark, J. Appl. Phys. **96**, 6827 (2004).

<sup>7</sup> A. B. Zorin, F.-J. Ahlers, J. Niemeyer, T. Weimann, H. Wolf, V. A. Krupenin, and S. V. Lotkhov, Phys. Rev. B **53**, 13682 (1996).

<sup>8</sup> V. A. Krupenin, D. E. Presnov, M. N. Savvateev, H. Scherer, A. B.

- Zorin, and J. Niemeyer, *J. Appl. Phys.* **84**, 3212 (1998).
- <sup>9</sup> A. N. Tavkhelidze and J. Mygind, *J. Appl. Phys.* **83**, 310 (1998).
- <sup>10</sup> N. M. Zimmerman, J. L. Cobb, and A. F. Clark, *Phys. Rev. B* **56**, 7675 (1997).
- <sup>11</sup> M. Kenyon, J. L. Cobb, A. Amar, D. Song, N. M. Zimmerman, C. J. Lobb, and F. C. Wellstood, *IEEE Trans. Appl. Supercond.* **9**, 4261 (1999).
- <sup>12</sup> B. E. Kane, *Nature* **393**, 133 (1998).
- <sup>13</sup> R. G. Knobel and A. N. Cleland, *Nature* **424**, 291 (2003).
- <sup>14</sup> C. D. Chen, Y. Nakamura, and J. S. Tsai, *Appl. Phys. Lett.* **71**, 2038 (1997).
- <sup>15</sup> T. A. Fulton and G. J. Dolan, *Phys. Rev. Lett.* **59**, 109 (1987).
- <sup>16</sup> N. M. Zimmerman, W. H. Huber, A. Fujiwara, and Y. Takahashi, *Appl. Phys. Lett.* **79**, 3188 (2001).